Synthesis and structural characterization of Eu(III)-doped $Zn_7Sb_2O_{12}$

A. C. S. Silva · G. G. Souza · M. A. L. Nobre · A. M. Pires

Abstract In addition to the lanthanide series elements, Europium is one of the chemical elements of greatest interest for the development of species with oxidation state +3 (III), which leads to interesting electronic transitions. In a general sense, their emission spectrum lines are narrow and sensitive to effects of the ligand field around metallic ions. This property allows the use of Eu(III) as a structural probe. In this work, samples of semiconductor $Zn_7Sb_2O_{12}$ and of solid solutions based on isoelectronically Eu(III)-doped $Zn_7Sb_2O_{12}$ with stoichiometry $Zn_{7-3x}Eu_{2x}Sb_2O_{12}$ were prepared. Both $Zn_7Sb_2O_{12}$ and $Zn_{7-3x}Eu_{2x}Sb_2O_{12}$ were synthesized via a chemical route using Pechini's method and characterized by Fourier transform infrared absorption vibrational spectroscopy (FTIR) and photoluminescence spectroscopy. In order to perform further spectral analyses, each spectrum was adjusted using a set of Gaussian functions. The FTIR spectrum analysis showed a slight band shift of the vibration mode assigned to the Sb–O bonding ascribed to the $[SbO_6]$ octahedron vibration. The theoretical fitting of the luminescence curves showed a broadening of the most intense emission peaks related to the transition Eu(III) $^5D_0 \rightarrow {}^7F_2$. As a whole, the results suggest that a less symmetric Eu(III) site occupation in inverse spinel structure may occur in sites close to the antimony octahedron, involving, however, non-substitutional site occupation.

A. C. S. Silva · G. G. Souza · M. A. L. Nobre · A. M. Pires (✉)
Depto. de Física, Química e Biologia, Faculdade Ciências e Tecnologia, Unesp Univ Estadual Paulista, P.O. Box 467, Presidente Prudente, SP 19060-900, Brazil
e-mail: anapires@fct.unesp.br

Introduction

Compounds based on elements belonging to the rare earth (RE) series, which include lanthanides, scandium, and yttrium, are excellent host structures for trivalent activator ions, as they exhibit enhanced luminescence [1], which is an essential feature for the design of functional luminescent materials based on morphological and structural studies. Lanthanide-doped semiconductor nanoparticles show a significant enhancement of radioactive transitions as a function of the decrease in particle size. As a consequence, improved emission efficiency of luminescent powders justifies an increased interest in the study of nanocrystalline materials with diameter sizes lesser than 100 nm [2]. Solid solutions based on the doping of the host structure with lanthanide elements exhibit luminescent emission due to internal 4f transitions. The f^n electrons of lanthanide ions are protected from interaction with the medium due to the shielding of the 5s and 5p outer full orbitals. Interesting transitions that yield visible emission light with relatively narrow bands, when compared with transition metals, are those with 4f (4f → 4f) configuration [3].

In particular, Eu(III) is one of the most interesting elements due to the fact that its main emissions in the visible range arise from the transition from the excited state $^5D_0$ (and the $^5D_{1,2,3}$ state) to the lower energy state $^7F_{0-6}$. Spectral lines usually are narrow and sensitive to the crystalline field around metallic ions. Among these transitions, in a general way, the electric dipole-allowed $^5D_0 \rightarrow {}^7F_2$ transition (0–2) is most intense in solid complexes (610 nm region). They are called hypersensitive because they are sensitive to the environment where the europium ion is located [3–5]. On the other hand, the $^5D_0 \rightarrow {}^7F_1$ transition (0–1) is magnetic dipole allowed; therefore, it does not undergo significant intensity changes

and occurs in the 590 nm spectral region, being practically independent of the formed ligand field. Thus, by establishing a relationship between the intensity of these two bands in the emission system, it is possible to predict features of the structural and/or chemical environment with which Eu(III) is associated, as well as its local symmetry. The existence of a band corresponding to the $^5D_0 \rightarrow {}^7F_0$ transition (0–0) indicates that Eu(III) is located in a site without an inversion center [2, 4, 5]. No splitting must not be involved in this 0–0 transition due to the effect of the crystalline field. Asymmetry in the contour of this band has been assigned to the presence of more than one Eu(III) emission sites [6]. Therefore, as a function of these electronic transitions in the incomplete orbital $4f^6$, the use of Eu(III) as an analytical structural probe is one of most important aspects in the spectroscopic study of Eu(III) luminescence [2–4].

In previous studies, Eu(III) was used as a dopant in the $Zn_7Sb_2O_{12}$ host structure in a non-isoelectronic medium and in varying preparation atmospheres. This host structure has an inverse spinel-type structure with eight tetrahedral sites randomly occupied by Zn^{2+} and 16 octahedral sites also randomly occupied by Sb^{5+} and Zn^{2+} [7, 8]. This phase exhibits an interesting common feature to spinel classes: its structure can dissolve a large amount of cations, including non-isovalent cations, which lends each phase a set of physical and chemical properties different from those of the original crystalline structure [9]. Oxide systems with this type of structure may have magnetic, electrical, catalytic, and sensing (temperature and gas) properties, and in the case of ceramics based on $Zn_7Sb_2O_{12}$, its electrical properties have been investigated aiming at applications such as temperature sensors [10–12]. Figure 1 shows the structural representation of the unit cell of the $Zn_7Sb_2O_{12}$ spinel.

In a broad sense, the addition of dopant cations to the $Zn_7Sb_2O_{12}$ host structure allows the modulation of its physical properties. These properties can be either enhanced
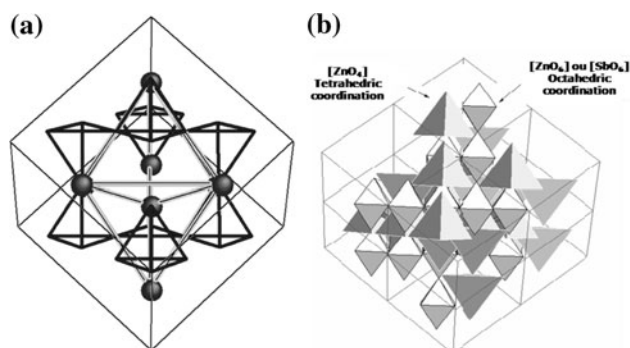
or inhibited, depending on the type and amount of dopant used. When Eu(III) is the chosen doping ion, monitoring its spectroscopic properties enables the investigation of the characteristics of its structure. The aim of this work was to prepare and perform the spectroscopic characterization of semiconductor $Zn_7Sb_2O_{12}$ and isoelectronically Eu(III)-doped $Zn_7Sb_2O_{12}$, according to the $Zn_{7-3x}Eu_{2x}Sb_2O_{12}$ stoichiometry. Additionally, another two solid solutions were non-isoelectronically synthesized, $Zn_{7-x}Eu_xSb_2O_{12}$ with x equal to 0.07, and $Zn_7Eu_{0.07}Sb_2O_{12}$ with excess Eu(III). Eu(III) will be used as a luminescent material in a potential probe of solid solutions, as a tool in elucidation of structural defects, as well as to investigate the influence of this ion on the structural and electrical characteristics of $Zn_7Sb_2O_{12}$. Therefore, the pure and Eu(III)-doped matrixes were characterized as to the influence of these ions on structural characteristics by monitoring spectroscopic properties.

Experimental

Pechini's method was used to synthesize pure $Zn_7Sb_2O_{12}$ and doped with 2–10 at.% substituting Zn(II) in an iso- or non-electronic way and 1 at.% of Eu(III) in excess according to the $Zn_{7-3x}Eu_{2x}Sb_2O_{12}$, $Zn_{7-x}Eu_xSb_2O_{12}$, and $Zn_7Eu_{0.07}Sb_2O_{12}$ stoichiometries, respectively. All metal oxides were solubilized under 80 °C by stirring in the presence of citric acid, ethylene glycol, and nitric acid solution and left to polymerize. For each mol of metal cation to be chelated, 3 moles of citric acid were used; the citric acid and ethylene glycol ratios were 60 and 40% by mass, respectively [7]. The beginning of polyesterification was identified by the decomposition of nitrate into NO_2, a brownish gas, and by an increase in the viscosity, yielding the polymeric resin. With the end of gas release, the organic phase degradation ended and the material was submitted to pre-calcination at 350 °C for 3 h. After this treatment, there was partial decomposition of the resin, forming the so-called puff (expanded resin), which consisted of a semi-charred powder. This material was ground and sieved in a 325-mesh sieve. Then, the powder was heated again to 1020 °C in air atmosphere for 1 h.

The $Zn_7Sb_2O_{12}$ nanoparticle size, shape, and crystallinity were characterized by transmission electron microscopy (TEM) at 200 kV in a Philips CM200 transmission microscope equipped with a Digital Spectrometer-Prism Princeton Gamma Tech PGT.

Structural characterization was carried out by XRD and data were collected in a RIGAKU® RINT2000 rotating anode diffractometer with Cu Kα radiation monochromatized by a curved graphite crystal; interval of 20°–80° (2θ), 0.02° (2θ) time per point of 0.3 s.

Fig. 1 a Structural representation by using tetrahedron and octahedron linkages, and **b** of the tetrahedra and octahedra in a unit cell of $Zn_7Sb_2O_{12}$ spinel. Figure generated by the software CaRIne Crystallography®

Luminescence spectroscopy at room temperature was performed by using an LS55 PerkinElmer Spectrofluorimeter equipped with a 9.9-W Xenon pulsed lamp and a R928 PMT photomultiplier for UV–Vis detection, and a filter wheel in the emission monochromator at 290, 350, 390, 430, and 515 nm. The samples were placed in a solid front face holder, and the excitation spectra were automatically corrected. Low temperature photoluminescence was measured in a FLUOROLOG3 ISA/Jobin–Yvon spectrofluorometer equipped with an R928P Hamamatsu photomultiplier and a 450-W ozone-free Xenon Lamp.

The chemical bond was investigated by FTIR spectroscopy. A spectrophotometer DIGILAB, model Excalibur, in diffuse reflectance mode was used. Samples were diluted in KBr in a ratio of 100:1 and pressed into homogeneous pellets. IR measurements were carried out with 100 scans in the range from 1000 to 400 cm^{-1} with 1 cm^{-1} resolution.
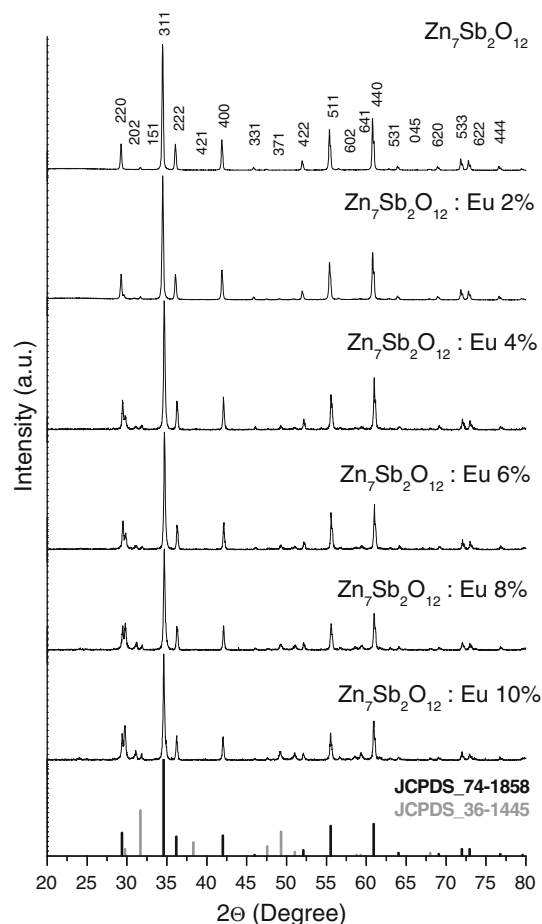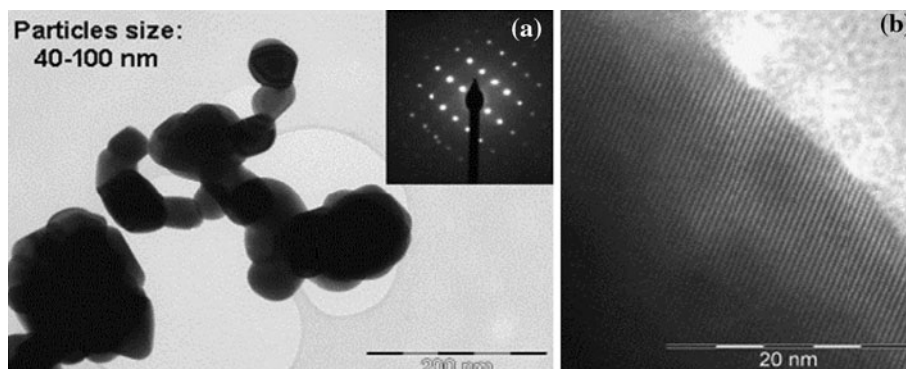
Results and discussion

TEM

TEM images of undoped sample, i.e., $Zn_7Sb_2O_{12}$, are shown in Fig. 2. The used synthesis route yielded small particle sizes in the range from 40 nm to 100 nm. The selected-area electron-diffraction (SAED) pattern of individual nanoparticles was obtained, Fig. 2a, top right inset, to evaluate their crystallinity. The well-defined SAED pattern confirmed that the sample is polycrystalline. The high-resolution TEM, Fig. 2b, shows the atomic plan distribution, confirming the good crystallization of a single nanoparticle.

X-ray diffraction

X-ray diffraction (XRD) data for all samples are shown in Fig. 3. Irrespective of whether the $Zn_7Sb_2O_{12}$ host structure is doped or not, all powders show the major

Fig. 3 XRD of undoped $Zn_7Sb_2O_{12}$ host structure and isoelectrically doped sample with 2–10 at.% Eu(III)

interplanar distances in accordance with the $Zn_7Sb_2O_{12}$ phase related to Powder Diffraction File PDF 74-1858 [13]. The existence of a small β-$Zn_7Sb_2O_{12}$ polymorphous phase fraction relative to Powder Diffraction File PDF 36-1445 [13] is also detected.

The XRD patterns do not show the formation of europium, zinc, or antimony oxides. However, an enlargement of the peak reflections with increasing Eu(III) percentage
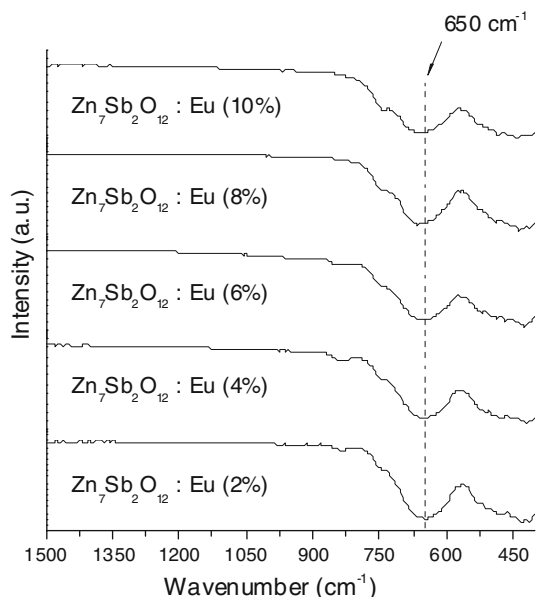

Fig. 2 TEM image of undoped $Zn_7Sb_2O_{12}$ **a** in panoramic view, top right insert shows the SAED pattern, and **b** high-resolution TEM, with a detailed view of the atomic plane distribution

can be noted. This fact suggests that the crystallinity may decrease with the increase in Eu(III) concentration in the host structure.

FTIR spectroscopy

Figure 4 shows FTIR spectra for samples of $Zn_7Sb_2O_{12}$ undoped and doped with Eu(III) in percentages from 2 to 10 at.%, in an isoelectronic way.

The broad band observed in the region of 650 cm^{-1} is assigned to the vibrational mode related to the octahedron of antimony. The visual inspection of the spectrum in Fig. 4 does not show band shifts assignable to the $[SbO_6]$ octahedron. Therefore, the curve was analyzed based on the theoretical adjustment. Prior to further analysis, the curves were converted to absorbance by adjustment with the Origin® Software using the supplied Gauss function and considering the vibrational absorption band assigned to the $[SbO_6]$ octahedron for all samples, Fig. 5. All graphs in Fig. 5 show that further adjustment is attained by using two or three Gaussians. The most intense component of all samples is shifted to the right; however, the calculated peak position seems to show a slight shift of the band characteristic of the vibrational mode assigned to the $[SbO_6]$ octahedron. To gain further insight on the spectral behavior of these samples, Fig. 5 also presents a curve fitting for samples prepared in a non-isoelectronic way and with excess Eu(III).

Table 1 shows the peak position values for all samples in the region from 550 to 800 cm^{-1} attributed to inverse spinel structure vibrational modes. The analysis of the peak positions from the curve fitting data shows a small shift of the band characteristic of the vibrational mode assigned to the $[SbO_6]$ octahedron.

Samples doped with 8 and 10 at.% Eu(III) and the one doped with 1 at.% Eu(III) in a non-isoelectronic way show a band shift (from 663.51 to 667.37 cm^{-1}) which may be indicative of local distortion caused by either higher Eu(III) concentrations or excess positive charge in the host structure.
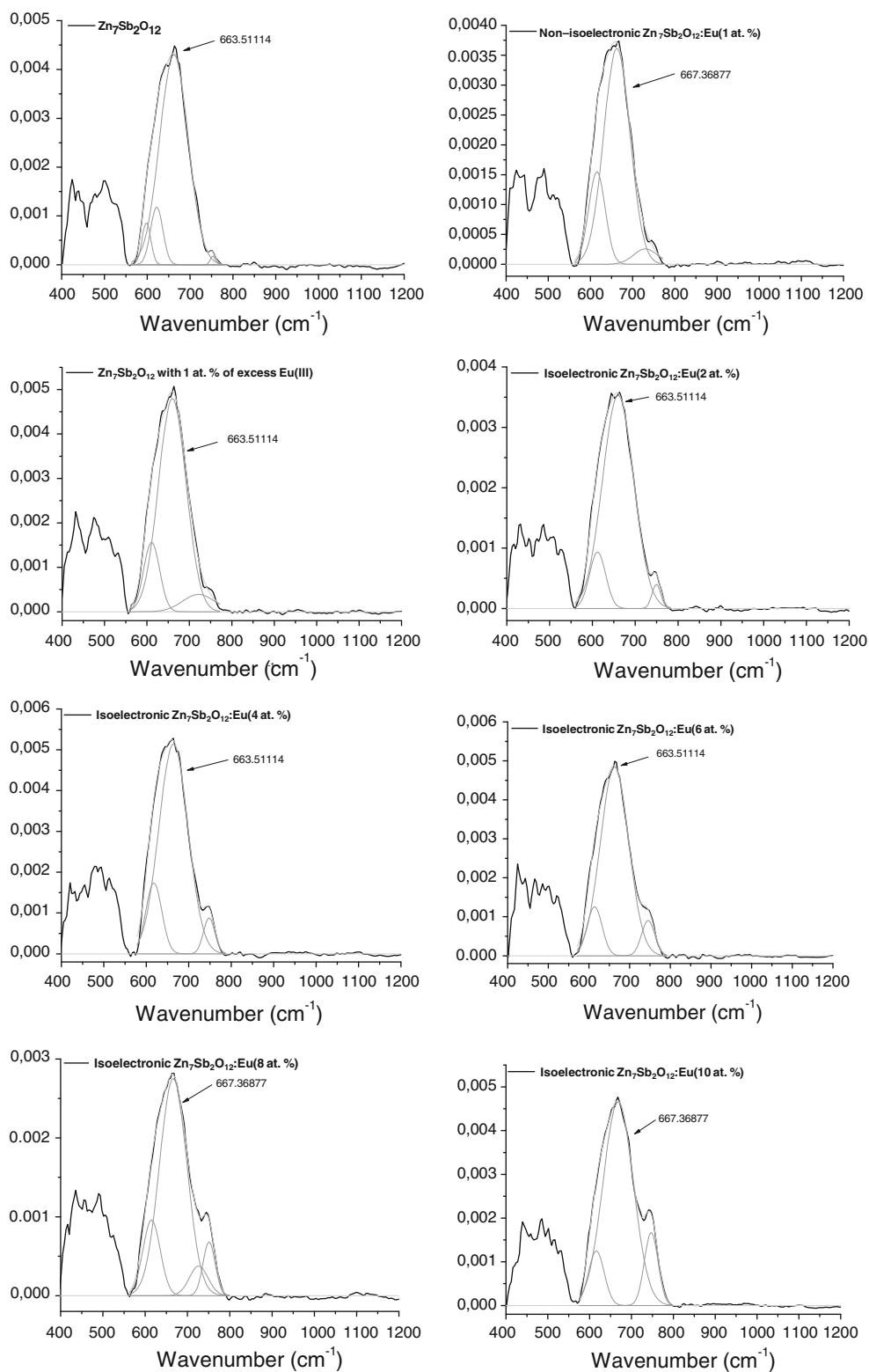
The development of some degree of lattice distortion as a function of the non-isovalent substitution of Zn(II) by Eu(III) is expected, since the ionic radius of the Eu(III) cation is larger than that of the Zn cation. As previously mentioned, the $Zn_7Sb_2O_{12}$ host structure exhibits an inverse spinel-type structure in which eight tetrahedral positions are occupied by Zn(II) and 16 octahedral positions are randomly occupied by both Sb(V) and Zn(II). Both Zn(II) and Sb(V) ions with coordination number (CN) equal to 6 have effective ionic radii of 0.74 and 0.60 Å, respectively, and Zn(II) with CN 4 has an effective ionic radius of 0.60 Å [14]. Therefore, we can expect that with an effective ionic radius equal to 0.95 Å [14] CN 6, Eu(III) would be large enough to cause a significant degree of distortion if an effective substitution of Sb(V) octahedral sites took place. As only a slight shift related to the vibrational mode of the $[SbO_6]$ octahedron is observed in all FTIR spectra, it is demonstrated that Eu(III) does not occupy Sb(V) octahedral sites; however, it must be very close to them.

Photoluminescence spectroscopy

The excitation and emission spectra measured at room temperature, Fig. 6, show the characteristic excitation transitions of Eu(III) obtained at set emission wavelengths of 612 and 627 nm. The 395 nm peak is assigned to the $^7F_0 \rightarrow {}^5L_6$ Eu(III) transition and the 466 nm and 477 nm peaks to the $^7F_0 \rightarrow {}^5D_2$ Eu(III) transition [15]. It must be emphasized that as all luminescence spectra were acquired at room temperature, the comparison of the adjusted curves is subject to the influence of peak broadening as a function of the vibrational components.

The spectra of all samples, Fig. 6, were recorded starting at 200 nm. Only part of the charge transfer band (CTB) was viewed below 225 nm. Since the relative intensity of the CTB is greater than the f–f transition peak intensities, Fig. 6 displays only the peaks above 380 nm for the magnification of the main region. The curves were fitted for the detected Eu(III) transitions using the Gauss function from the Origin® software for all excitation spectra in Fig. 6. These results show that in the case of peaks assigned to the $^7F_0 \rightarrow {}^5D_2$ transition, the component with the highest intensity is slightly shifted, which indicates that Eu(III) is occupying different sites. According to the FTIR

Fig. 4 FTIR spectra of $Zn_7Sb_2O_{12}$ isoelectrically doped with 2–10 at.% Eu(III)

Fig. 5 Curve fitting for FTIR spectra using Origin® Software

discussion, the small shift of the band characteristic of the vibrational mode assigned to the [SbO$_6$] octahedron indicates that Eu(III) does not substitute the Sb cation in the octahedron, but that it must be close enough to cause a slight distortion of the local structure and that it may be

occupying slightly different vacancy sites, which can justify the small shift of the $^7F_0 \rightarrow {}^5D_2$ Eu(III) transition.

From the emission spectra of all doped samples under 466 nm excitation, Fig. 7, it is possible to detect the characteristic Eu(III) set of transitions $^5D_0 \rightarrow {}^7F_0$,
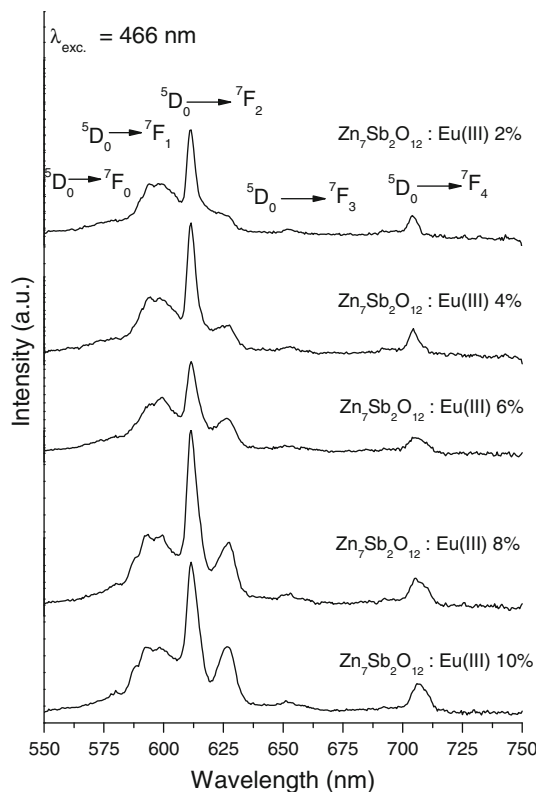
Table 1 Maximum FTIR peak values in the range from 550 to 800 cm^{-1} assigned to vibrational modes related to the [SbO$_6$] octahedron of the spinel structure of pure and doped samples

Sample	Peak maximum (cm^{-1})
Zn$_7$Sb$_2$O$_{12}$	663.51
Non-isoelectronic Zn$_7$Sb$_2$O$_{12}$:Eu(1 at.%)	667.37
Zn$_7$Sb$_2$O$_{12}$ with 1 at.% of excess Eu(III)	663.51
Isoelectronic Zn$_7$Sb$_2$O$_{12}$:Eu (2 at.%)	663.51
Isoelectronic Zn$_7$Sb$_2$O$_{12}$:Eu (4 at.%)	663.51
Isoelectronic Zn$_7$Sb$_2$O$_{12}$:Eu (6 at.%)	663.51
Isoelectronic Zn$_7$Sb$_2$O$_{12}$:Eu (8 at.%)	667.37
Isoelectronic Zn$_7$Sb$_2$O$_{12}$:Eu (10 at.%)	667.37

$^5D_0 \rightarrow {}^7F_1$, $^5D_0 \rightarrow {}^7F_2$, $^5D_0 \rightarrow {}^7F_3$, and $^5D_0 \rightarrow {}^7F_4$ with maximum peaks at 580, 596, 611, 653, and 706 nm, respectively [15].
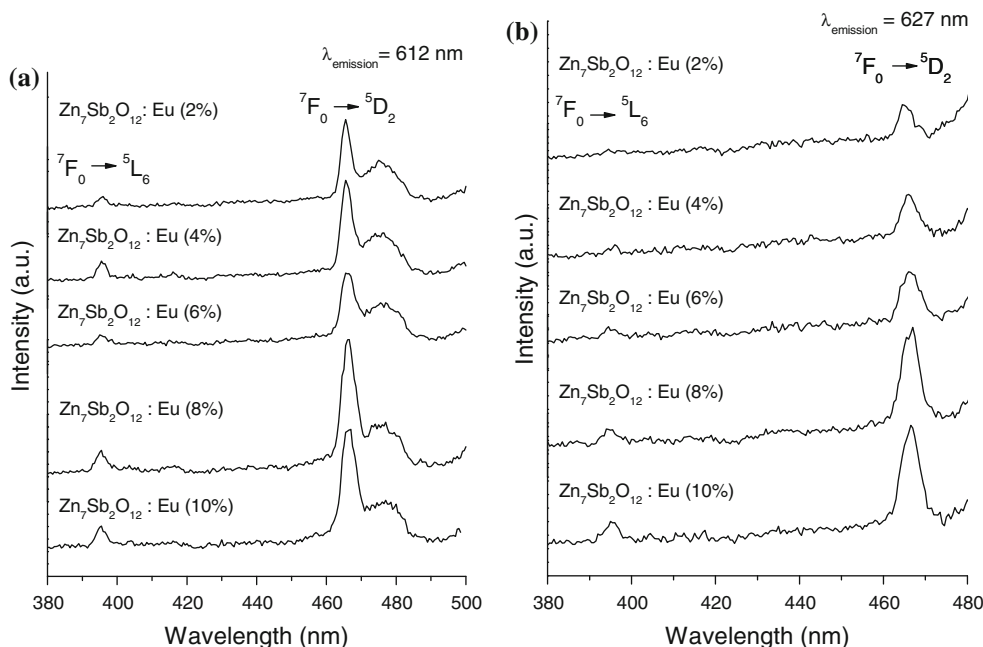
Similarly to the infrared spectra analysis, the emission spectra were successfully fitted for analysis using the Origin® Software, specifically the emission range assigned to the $^5D_0 \rightarrow {}^7F_2$ Eu(III) transition for isoelectronically doped samples, and the two samples doped in a non-isoelectronic way and with excess Eu(III), Fig. 8.

The analysis of Fig. 8 shows that the positions of all peaks are very similar. However, there is a clear variation of relative intensity, which is greater for the sample isoelectronically doped with 10 at.% Eu(III). The plot of half height width versus Eu(III) percentage shows that there is a peak broadening as a function of the increase in the Eu(III) content. This event suggests that less symmetric sites of the spinel structure may be occupied by Eu(III). As previously
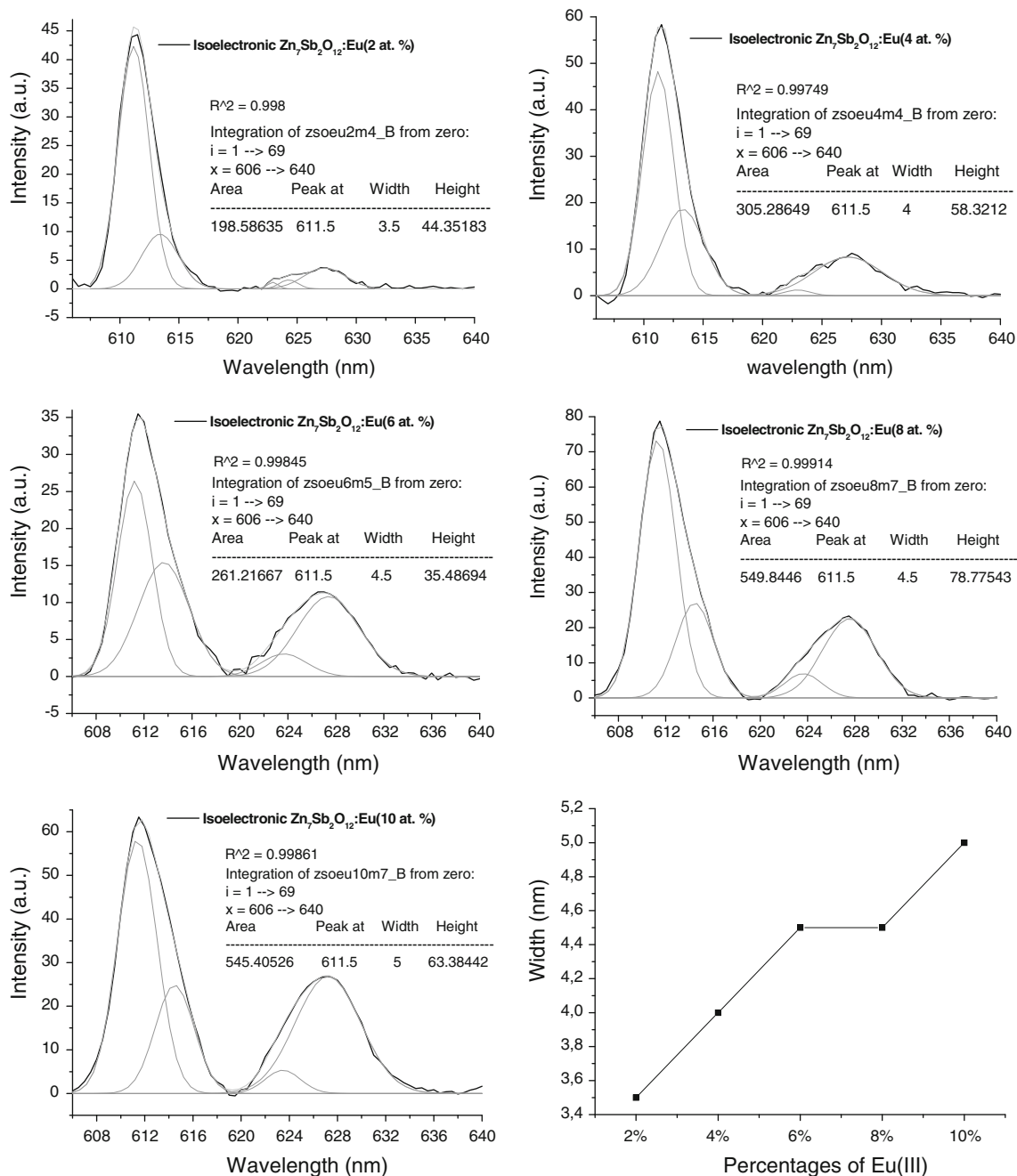

Fig. 7 Emission spectra of doped samples under 466 nm excitation at room temperature

mentioned, the ionic radius of Eu(III) is greater than those of the ions of the host structure, independent of the coordination number. Therefore, the peak broadening with the increase in the Eu(III) concentration may be due to vacant

Fig. 6 Excitation spectra at room temperature **a** λ_{em} at 612 nm and **b** λ_{em} at 627 nm

Fig. 8 Fitted curves of the emission spectra at room temperature under 466 nm excitation related to the $^5D_0 \rightarrow {}^7F_2$ transition set for all doped samples in an isoelectronic way. The graph of half height width versus Eu(III) percentage is also shown
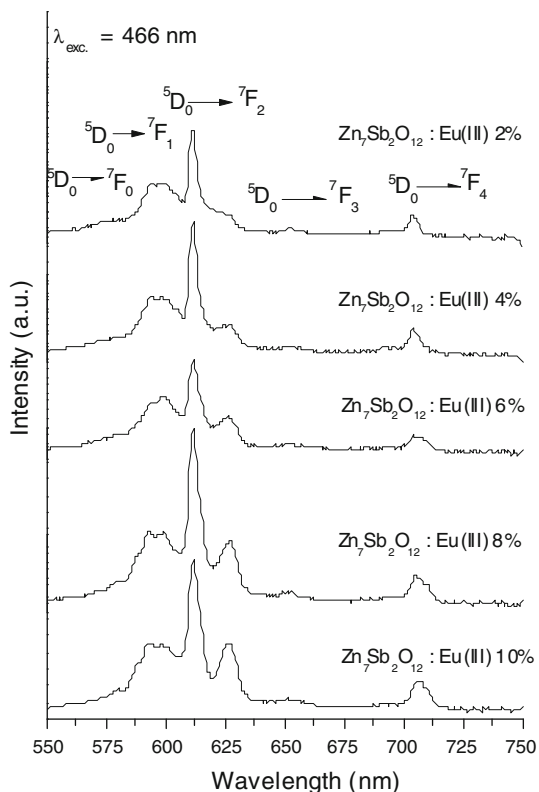
site occupation and not necessarily to the substitution of Zn(II) or Sb(V) by Eu(III).

Figure 9 shows the emission spectra of the samples isoelectronically doped with 2 at.% of Eu(III) and with 1 at.% in a non-isoelectronic way at room and low temperatures. It is possible to observe that the low temperature measurement provides better solved spectra; however, the band broadening ascribed to the vibrational component is

not so high, which supports the previous considerations on site occupation by Eu(III).

Conclusion

XRD data confirmed the formation of the $Zn_7Sb_2O_{12}$ phase. The Eu(III) concentration increase leads to a

Fig. 9 Emission spectra for samples doped with 2 at.% of Eu(III) in an isoelectronic and 1 at.% in a non-isoelectronic way at room and low (liquid nitrogen) temperatures under 465 nm excitation

decrease in crystallinity due to a random local distortion. The FTIR spectra corroborated that local distortion occurs with increasing Eu(III) doping concentration, and also that Eu(III) must not substitute the Sb in the $[SbO_6]$ octahedron. All characteristic excitation and emission transitions of the Eu(III) cation were identified. The detailed analysis of the theoretically fitted emission curve also corroborated the

position of Eu(III) ions in the crystalline lattice by occupation of less symmetric Eu(III) sites. Since inverse spinel structure exhibits a great number of vacant sites, Eu(III) shows a tendency to occupy sites closer to the antimony octahedron; involving, however, non-substitutional doping.

References

1. Gasparotto G, Cebim MA, Goes MS, Lima, SAM, Davolos MR, Varela JA, Paiva-Santos CO, Zaghete MA (2009) J Appl Phys 106:063509-1-5
2. Strek W, Deren P, Bednarkiewicz A, Zawadzki M, Wrzyszcz J (2000) J Alloys Compd 300–301:456
3. Barros BS, Melo PS, Gama L, Alves-Jr S, Fagury-Neto E, Kiminami RHGA, Costa ACFM (2005) Rev Cerâmica 51:63
4. Nassar EJ, Ciuffi KJ (2003) Quim Nova 26:674
5. Leonard JP, Gunnlaugsson T (2005) J Fluoresc 15:585
6. Nassar EJ, Serra AO, Aguiar EFA (1998) Quim Nova 21:121
7. Nobre MAL, Lanfredi S (2001) Mater Lett 50:322
8. Gouveia DS, Soledade LEB, Paskocimas CA, Longo E, Souza AG, Santos IMG (2005) Mater Res Bull 8:213
9. Gama L, Vila C, Campaneri RL, Paiva-Santos CO, Varela JA, Longo E (2000) Rev Cerâmica 46:220
10. Nobre MAL, Lanfredi S (2003) Mater Res Bull 6:151
11. Pu Y, Chen W, Chen S, Langhammer HT (2005) Rev Cerâmica 51:214
12. Peverari C, Pires AM, Gonçalves RR, Serra AO (2005) Eclética Química 30:59
13. Powder Diffraction File PDF-2 database sets 1-44, Pennsylvania Joint Committee on Powder Diffraction Standards, International Center for Diffraction Data, copyright 1988, PDG numbers 74-1858 and 36-1445 (CD-ROM)
14. Shannon RD (1976) Acta Crystallogr A A32:751
15. Pires AM, Davolos (2001) Chem Mater 13:21